Journal of Power Sources 226 (2013) 127–133

Contents lists available at SciVerse ScienceDirect

Journal of Power Sources

journal homepage: www.elsevier.com/locate/jpowsour

Optimization of Al_2O_3–glass composite seals for planar intermediate-temperature solid oxide fuel cells

Xiaopeng Wang, Dong Yan, Dawei Fang, Jun Luo, Jian Pu, Bo Chi, Li Jian*

Center for Fuel Cell Innovation, School of Materials Science and Engineering, State Key Laboratory of Material Processing and Die & Mould Technology, Huazhong University of Science & Technology, Wuhan, Hubei 430074, China

HIGHLIGHTS

- Al_2O_3–HGS composite seals were prepared by tape-casting.
- Leakage was tested at various temperatures, N_2 pressures and compressive loads.
- Thermal cycle sealing performance of AG50 was evaluated between 200 and 750 °C.
- Single cell was tested at 750 °C with H_2 fuel, air oxidant and AG50 seal.

ARTICLE INFO

Article history:
Received 10 October 2012
Accepted 19 October 2012
Available online 6 November 2012

Keywords:
Solid oxide fuel cell
Glass–ceramic composite seals
Leak rate
Thermal cycling capability
Glass content

ABSTRACT

Al_2O_3–glass composite seals are fabricated by tape casting Al_2O_3 and HGS glass powder mixtures with glass contents ranging from 20 to 60 wt%. Their leaking performance is evaluated for various temperatures, gas pressures and compressive loads. The seal with optimized glass content is subjected to thermal cycling and single-cell tests to investigate the viability of the seal. The sealing performance of the seal is significantly improved by increasing the glass content in the composite seal; the seal containing 50 wt% glass (AG50) shows the best sealing performance among the studied compositions. Increasing the testing gas pressure or decreasing the testing temperature and compressive load increase the leak rate of the seal. After 25 thermal cycles between 750 and 200 °C, the leak rate of the AG50 seal is still below 0.021 sccm cm^{-1} under the conditions of 750 °C, a compressive load of 0.12 MPa and a testing gas pressure of 3.5 kPa to 10.5 kPa. Using the AG50 seal, a high open circuit voltage of above 1.16 V after 6 thermal cycles is achieved for a 10 × 10 cm^2 anode-supported single cell (active area of 9 × 9 cm^2), which demonstrates the applicability of the AG50 seal in practical SOFC operations.

1. Introduction

Solid oxide fuel cells (SOFCs) are a promising electrochemical device that generates electrical power in an efficient and environmentally friendly manner by converting chemical energy in fossil or hydrocarbon fuels. Planar intermediate-temperature SOFCs have attracted much attention in the past decade because their characteristically lower operating temperature reduces manufacturing/maintenance costs and allows the use of metallic interconnects. In planar SOFCs, the seal is a crucial component located between the planar cell and the metallic interconnect in a stack that prevents the mixing of fuel and oxidant gases. Thus, in addition to the required sealing performance, the sealing materials also must be chemically stable, electrically insulating, and chemically and thermally compatible with the contacted components in both oxidizing and reducing dual environments. With the growing interest in SOFCs as a sustainable source of energy, significant efforts have been made to develop sealing materials [1–5], which are mechanistically classified into two types: rigid and compressive seals [6–8].

Materials for rigid seals are usually glasses or dense glass–ceramics [9], which "glue" the components together by forming a rigid bond and provide hermetic sealing. Above the glass softening temperature, they soften and flow to form an intimate contact with surface of the components to be sealed and maintain the sealing performance. However, they harden and tend to detach from sealing surfaces or crack if their coefficient of thermal expansion (CTE) differs from those of the contacting components. Therefore, the CTE of the rigid sealing materials must be carefully tailored by optimizing their composition [10,11]. Furthermore, glass materials are brittle in nature and susceptible to fracturing under tensile stresses, which may damage the integrity of the seal and compromise its sealing performance during long-term operations,

* Corresponding author. Tel.: +86 27 8755 7694; fax: +86 27 8755 8142.
E-mail address: lijian@hust.edu.cn (L. Jian).

0378-7753/$ – see front matter © 2012 Elsevier B.V. All rights reserved.
http://dx.doi.org/10.1016/j.jpowsour.2012.10.084

especially thermal cycles [12,13]. Nevertheless, glass sealing materials possess a unique self-healing capability [13–16]; tiny cracks formed during thermal cycles can self-heal at SOFC operating temperatures, recovering the mechanical properties and sealing performance of the seal. This self-healing feature is desired for rigid seals to improve sealing performance during thermal cycling [17–19].

Compressive seals function under an external compressive load that is vertically applied across the sealing surfaces. The seal is not rigidly bonded to the contacting surfaces; therefore, the thermal expansion coefficients for the seal and the contacting components may differ, which is a unique advantage of the compressive seal. Sang et al. [20] and Dai et al. [21] have developed Al_2O_3-based compressive seals, which are made from highly inert Al_2O_3 powder containing Al additives by low-cost tape casting technology. Such compressive seals have shown adequate sealing performance and excellent thermal cycling capability and do not react with the contacting components. However, their mechanical strength is a potential issue, as the seals are basically a closely packed powder bed without sintering at intermediate temperatures. In addition, the sealing interface tends to be leaking if the stack components are not perfectly flat, causing a non-uniform loading on the entire seal. To combine the advantages of both rigid and compressive seals while avoiding their individual disadvantages, Ye et al. [22] developed a glass-based composite seal that contained 30 wt% fine Al_2O_3 powder and 70 wt% glass powder. The seal demonstrated a thermal cycle leakage below 0.01 sccm cm^{-1} under a compressive load of 0.14 MPa at 750 °C. However, the extremely high glass content in this seal may result in excessive shrinkage, which in turn may lead to failure when the applied load on the seal is not adequately uniform. Ideally, the glass component should be flowable, compressible and self-healing at the operating temperature, with the Al_2O_3 component acting as a backbone to prevent excessive glass shrinkage and seal fracture upon cooling. With increasing glass content in the composite seal, the seal may gradually evolve from a compressive- to a rigid-type seal. The purpose of this study is to optimize the composition of the composite seal by investigating the effects of various Al_2O_3-to-glass weight ratios (above 30:70) on leak rate, microstructure, thermal cycling capability, compressibility, compatibility and performance in a single-cell test.

2. Experimental

2.1. Seal preparation

Powder mixtures of Al_2O_3 from Almatis and glass (HGS) from New Hua Guang were employed for the fabrication of the glass–ceramic composite seals by tape casting. The molar composition of the glass is approximately 8.6% B_2O_3–12.9% BaO–21.2% MgO–13.6% ZnO–43.7% SiO_2, and the glass transition temperature T_g is approximately 680 °C. The original average particle sizes of the Al_2O_3 and HGS glass powder are approximately 1.2 and 22.8 μm, respectively, as determined by a laser particle size analyzer (JL-1155, Chengdu Jingxin Powder Testing, China). After ball milling for 24 h, the difference in particle size of the Al_2O_3 and HGS glass powder becomes much smaller (Fig. 1), which will facilitate the tape casting process. By following previously described procedures [20–22], slurries of the powder mixture were prepared and tape cast using an alcohol and xylene mixture as the solvent, Menhaden fish oil as the dispersant, polyvinyl butyral as the binder and butyl benzyl phthalate as the plasticizer. Square window frame seal specimens with an outside dimension of 7 × 7 cm and an inside dimension of 5 × 5 cm were cut out of the dried tape (0.4 mm thick) for the leak test. The Al_2O_3-to-HGS weight ratios in the tape were 80:20, 70:30, 60:40, 50:50 and 40:60, and the corresponding specimens were designated as AG20, AG30, AG40, AG50 and AG60, respectively.

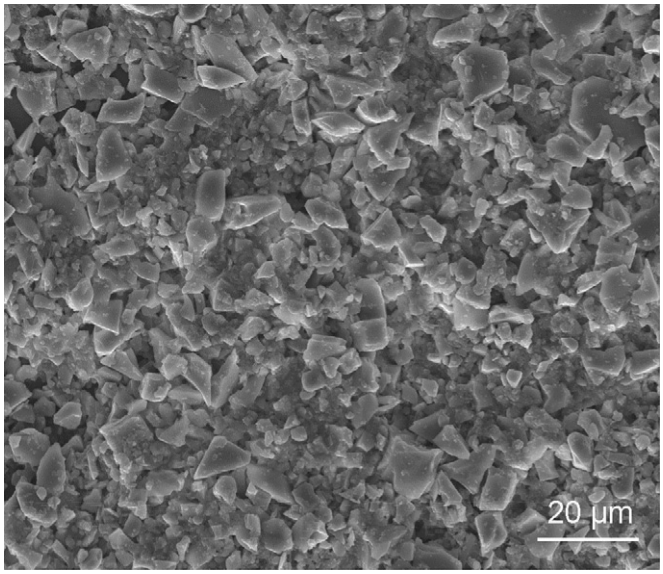

Fig. 1. SEM morphology of the Al_2O_3–HGS glass powder mixture (weight ratio 50:50) used for the fabrication of composite seals by tape casting.

2.2. Sealing performance and thermal cycling capability evaluation

To evaluate the sealing and thermal cycling performance, the prepared window frame specimens were tested in the leak tester depicted in Reference [20]. Clamped between two SUS 430 stainless steel plates under an external load, the specimen was programmably heated in a furnace to the testing temperatures. The testing gas, N_2, was injected into the empty space within the window frame specimen at various pressures via a hole at the center of the bottom plate using a precision flow meter (Omega Engineering, accuracy of 0.001 sccm), which indicates the leakage of the specimen. The heating program was chosen according to the results of thermogravimetric analysis for the tape. Thus, the window frame specimen was heated slowly to 200 °C at 1.5 °C min^{-1}, where it remained for 60 min to allow the organic additives to burn out gradually. The specimen was then further heated to testing temperatures of 700, 750 or 800 °C at 2 °C min^{-1}. The leak rate was examined at various N_2 pressures between 3.5 and 21 kPa under different compressive loads of 0.07, 0.12 and 0.17 MPa. The thermal cycling was carried out between 200 and 750 °C under a compressive load of 0.12 MPa and various N_2 pressures, and the leakage at 200 and 750 °C was recorded for each cycle. The morphology and phases of the post-test specimens were examined by scanning electron microscopy (SEM, Quanta 200) and X-ray diffraction (XRD, X'Pert Pro).

2.3. Seal compressibility

At the operating temperature, the glass in the seal is expected to be capable of "flowing" to fill the pores created by burnt-out organic additives and self-heal the cracks that may form during thermal cycles, allowing the seal to conform well to the contours of the sealing surfaces. To understand the deformability or compressibility of the seal with various glass contents, it was sandwiched between two SUS 430 plates (20 × 20 × 1 mm) and compressed under a compressive load of 0.12 MPa at room temperature for 2 h and then at 750 °C for another 2 h. Neglecting

the deformation of the steel plates, the compressibility of the seal was calculated by the following equation:

$$\text{Compressibility} = \frac{\text{Final thickness } H_2 - \text{Initial thickness } H_1}{\text{Original thickness } H_0} \quad (1)$$

where H_0 is the original thickness of the seal, H_1 is the thickness of the "sandwich" after room temperature compression, and H_2 is the thickness of the "sandwich" after compression at 750 °C. The heating program used was the same as that for the leak test.

2.4. Interface examination

The glass–ceramic composite seal is applied in a planar SOFC stack between the metallic interconnect and the cell; therefore, there are two possible leak paths associated with the seal, i.e., leaking through the body of the seal and leaking through the contact interface. The interface is more vulnerable to leaking, and the leaking rate through the interface is several orders of magnitude higher than that through the body of the seal [17,23], which implies the importance of the interface in the sealing performance. To simulate the performance of the seal in a SOFC stack, the seal was placed between a SUS 430 plate (20 × 20 × 1 mm) and a piece of anode-supported cell and then heated at 750 °C under a compressive load of 0.12 MPa for 2 h. The interfaces after the test were examined by SEM.

2.5. Seal evaluation in single-cell test

For the single-cell test, square window frame specimens with a periphery dimension of 10 × 10 cm and a width of 1 cm were prepared for sealing on both the anode and cathode sides of the cell. The testing jig was made of SUS 430 stainless steel plates with gas distribution channels; and a cell with an active area of 9 × 9 cm^2 was fabricated in-house. The cell test was conducted at 750 °C under a compressive load of 0.10 MPa using pure H_2 as the fuel and air as the oxidant; the power curve and thermally cycled durability performance were obtained from the test.

3. Results and discussion

The leak rates of the prepared seals (AG20 to AG60) were measured at N_2 pressures between 3.5 and 21 kPa and temperatures of 700, 750 and 800 °C under different compressive loads of 0.07, 0.12 and 0.17 MPa at 750 °C in air. The leak performance of the seal was affected by all of these parameters. Fig. 2 shows the leak performance variation of each specimen with N_2 pressure under a constant compressive load of 0.12 MPa, which indicates that the leak rate of the seal decreased as the glass content increased and the N_2 pressure decreased. For glass contents below 50 wt%, the leak performance of the seal was equivalent to or worse than that of the Al_2O_3–30 wt% Al composite seal [20]. However, for glass contents at or above 50 wt%, the leakage dropped significantly to below 0.008 sccm cm^{-1} and was barely affected by the N_2 pressure. Fig. 3 presents the cross-sectional microstructure of the frame seals with various glass contents after the leak test. The seal was gradually densified with the increase in glass content by the coalescence of glass particles and glass encapsulation of Al_2O_3 particles. In the AG20, AG30 and AG40 seals, the glass particles were not fully coalesced and the Al_2O_3 particles were not completely encapsulated due to the insufficient glass content. However, in the AG50 and AG60 seals, pores were barely observable, which explains the extremely low leakage observed.

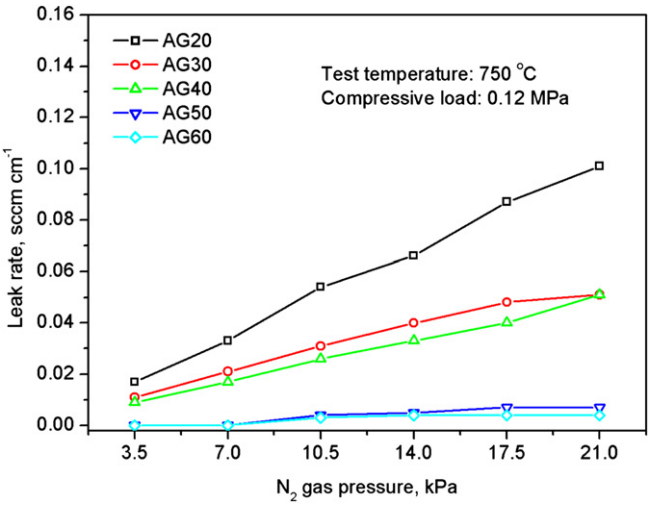

Fig. 2. Dependence of the leak rate on the N_2 gas pressure for tape-cast Al_2O_3–glass composite seals with various glass contents at 750 °C and a 0.12 MPa compressive load.

T_g of this glass is approximately 680 °C; thus, it is expected to become soft and flowing at the testing temperature of 750 °C, allowing it to eliminate the pores in the compressed seal. The compressibility of the prepared seals at 750 °C is demonstrated in Fig. 4, which confirms that the AG50 and AG60 seals were highly compressible at the testing temperature due to the softness and flowability of the glass.

The above results indicate that the higher the glass content in the seal, the better the sealing performance is. Nevertheless, seal breakage tends to occur when the glass content in the seal is high. The cast tape seal is porous after debindering and densifies in situ during operation; it is also prone to breaking in a SOFC stack when the applied compressive load is not perfectly uniform.

To clarify whether such seal breakages may occur under the operating conditions normally applied to the stack, further measurements were made using the AG50 seal, which was considered to have the optimal composition among the seals studied. Fig. 5 shows the leak rate of the AG50 seal under various operating conditions with temperatures varying from 700 to 800 °C, N_2 pressures from 3.5 to 21 kPa and compressive loads from 0.07 to 0.17 MPa. These parameter ranges cover the operating conditions of a typical planar intermediate-temperature SOFC stack. The results indicate that the leak rate at constant N_2 pressure decreased as the operating temperature increased from 700 to 800 °C (Fig. 5a) and the compressive load increased from 0.07 to 0.17 MPa (Fig. 5b). The leak rate increased as the N_2 pressure increased from 3.5 to 21 kPa at constant temperature and compressive load. The highest leak rate was observed under conditions of 700 °C and a 0.12 MPa compressive load; however, it was only 0.016 sccm cm^{-1}, which was far below the conventional requirement for a seal used in intermediate-temperature SOFC stacks. To further understand the sealing performance of the AG50 seal, it was thermally cycled between 200 and 750 °C for up to 25 cycles, which is more than the conventionally required number of thermal cycles for stationary SOFC stacks. Fig. 6 shows the leak rate of AG50 seal after each thermal cycle under the most frequently used stack operating condition of 750 °C, a gas pressure of 3.5–10.5 kPa and a 0.12 MPa compressive load. The leak rate increased moderately with the number of thermal cycles due to thermal strain accumulation; however, the highest leak rate was still only 0.021 sccm cm^{-1}, which was far below the well-accepted level of 0.040 sccm cm^{-1} and demonstrated the

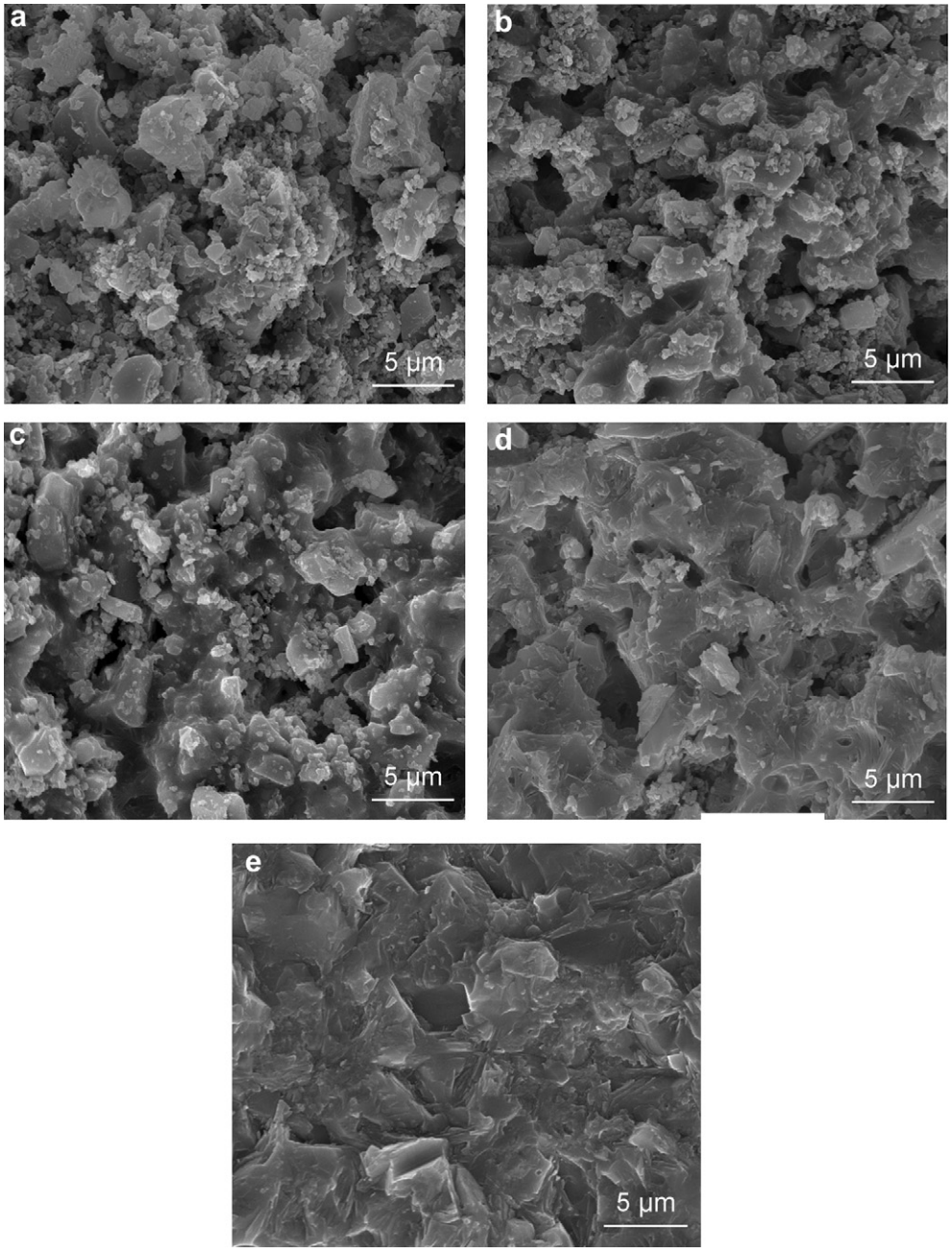

Fig. 3. SEM microstructure of Al_2O_3–HGS glass composite seals after leak testing at 750 °C, a 0.12 MPa compressive load and N_2 gas pressures ranging from 3.5 to 21 kPa: a) AG20, b) AG30, c) AG40, d) AG50 and e) AG60.

excellent thermal cycling capability of the AG50 seal. Fig. 7 displays the XRD patterns of the AG50 seals leak-tested at 700, 750 and 800 °C for 2 h and the XRD pattern of the AG50 seal thermally cycled between 200 and 750 °C. The glass phase was stable at 700 °C, but it reacted with Al_2O_3 to form $BaAl_2Si_2O_8$ and crystallized (indicated by the small, unidentified peaks) at or above 750 °C. However, the phase change in the AG50 seal did not degrade its sealing performance beyond acceptance.

To prove its viability in the cell application, the AD50 seal was adopted in the performance testing of a 10 × 10 cm^2 single cell (active area of 9 × 9 cm^2) at 750 °C as described in detail above. The power and *I*–*V* curves of the cell revealed a high open circuit voltage (OCV) of ~1.18 V and a high power density of 745 mW cm^{-2} at 988 mA cm^{-2} (Fig. 8). Furthermore, this cell was thermally cycled 6 times between 750 and 200 °C over more than 100 h of testing, in which the OCV varied between 1.16 and 1.19 V, and the cell performance at 500 mA cm^{-2} decreased slightly from 0.864 V to 0.794 V (Fig. 9). These high thermally cycled OCVs suggest that the AG50 seal is thermally cyclable and suitable for SOFC applications. Fig. 10 exhibits SEM micrographs of the interfaces of AG50 seal/SUS 430 stainless steel plates (simulating the interconnect) and AG50 seal/anode support (NiO–YSZ) after 2 h at 750 °C. The AG50 seal was well adhered to the cell and the "interconnect" and sealed the primary leak path, demonstrating its excellent sealing performance. The SUS 430 stainless steel was slightly oxidized, which usually leads to the formation of an oxide scale containing Cr_2O_3 and $MnCr_2O_4$ [24]. Thermal cycling may cause damage on the interface due to some mismatch in the CTE between the seal and

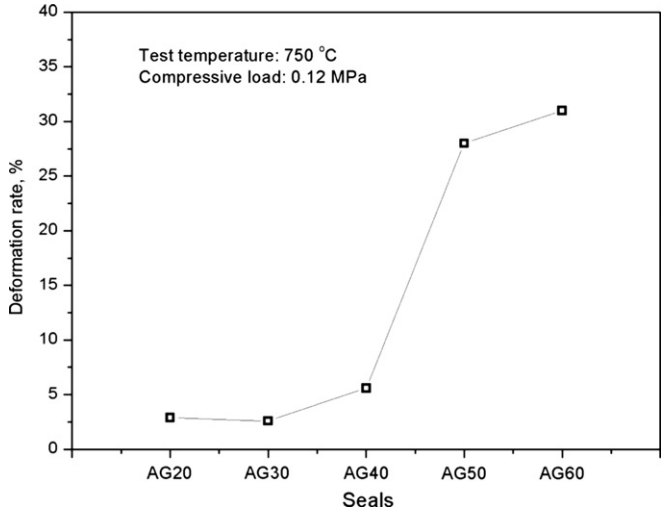

Fig. 4. Compressibility of the composite seals with various glass contents tested at 750 °C and a 0.12 MPa compressive load.

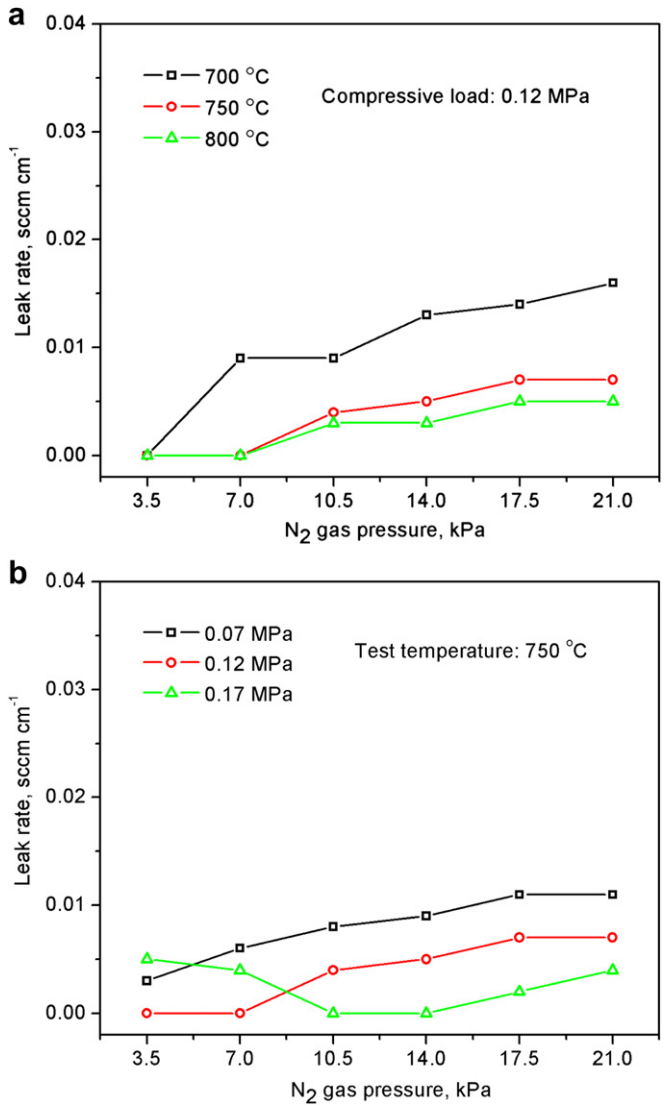

Fig. 5. Dependence of sealing performance on N_2 gas pressure for the AG50 seal tested for a) temperatures ranging from 700 to 800 °C and b) compressive loads ranging from 0.07 to 0.17 MPa.

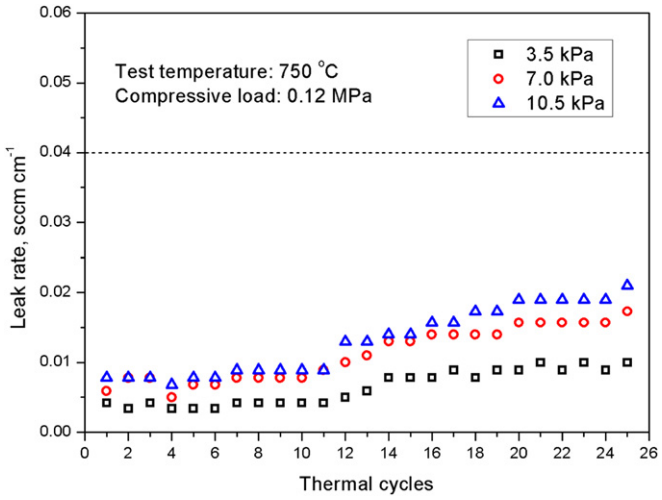

Fig. 6. Variation of leak rate of the AG50 seal with the number of thermal cycles. Thermal cycling was conducted between 200 and 750 °C, and the leak rate was measured after each cycle at 750 °C with a 0.12 MPa compressive load and N_2 gas pressures ranging from 3.5 to 10.5 kPa.

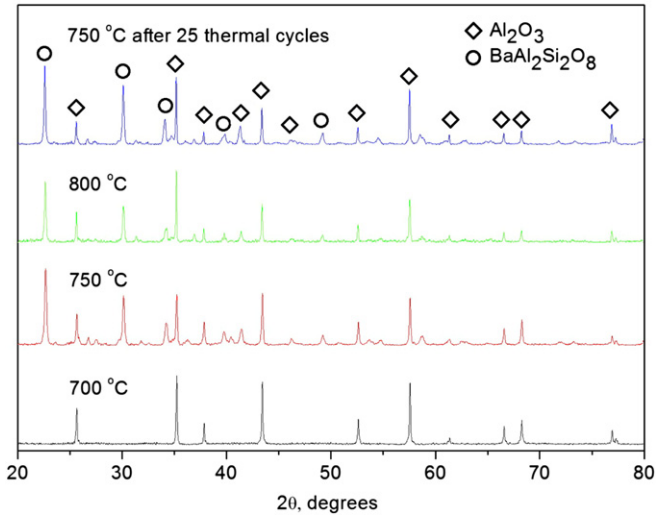

Fig. 7. XRD patterns of the AG50 seals leak-tested at 700, 750 and 800 °C for 2 h and thermally cycled between 200 and 750 °C, showing $BaAl_2Si_2O_8$ formation and glass crystallization at 750 °C and above.

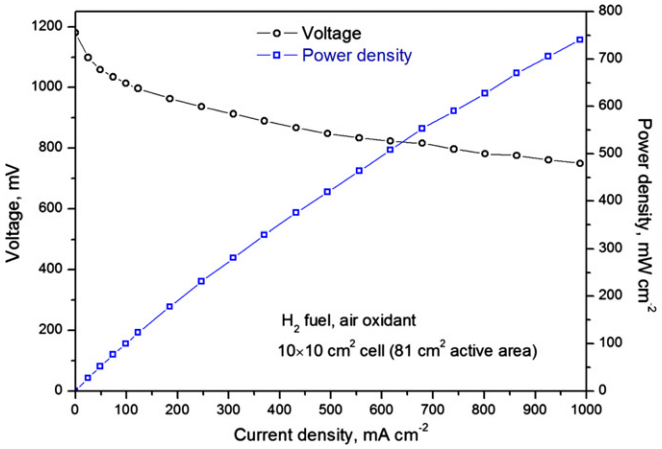

Fig. 8. *I–V* and power curves of a single cell tested at 750 °C using H_2 as the fuel, air as the oxidant and AG50 as the seal.

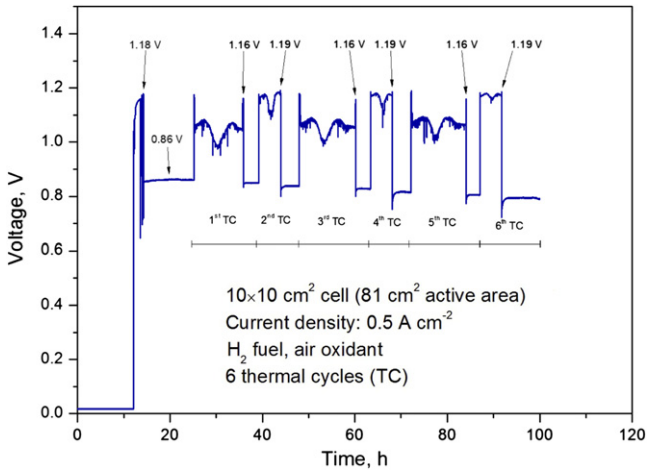

Fig. 9. Thermal cycling durability of a single cell tested using H_2 as the fuel, air as the oxidant and AG50 as the seal.

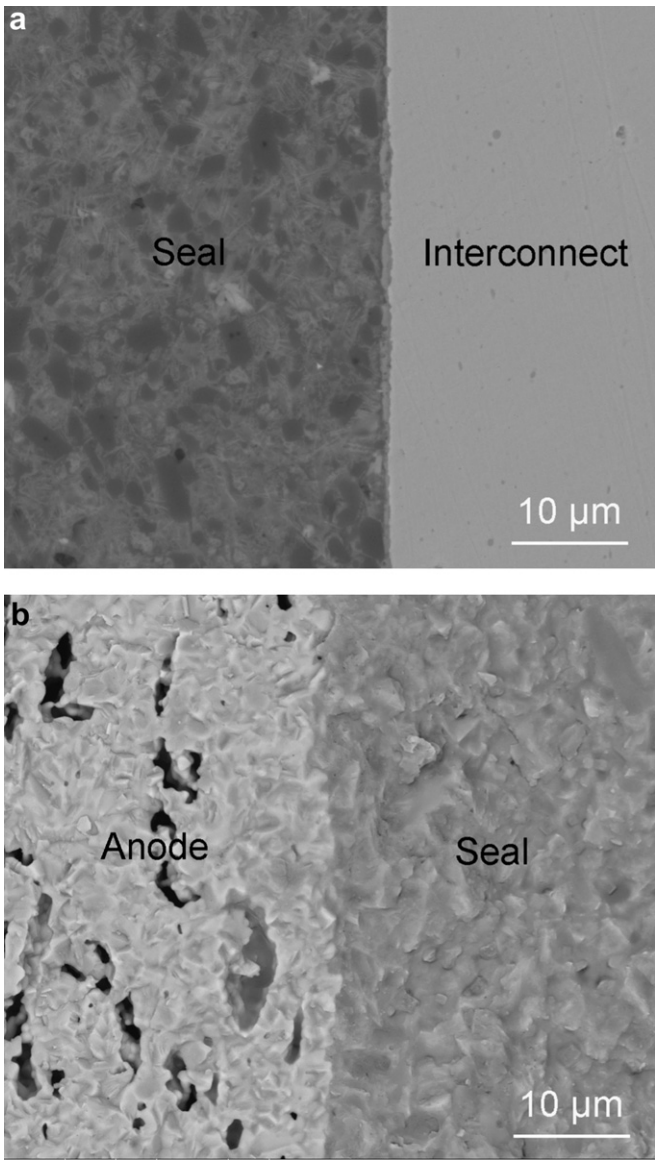

Fig. 10. SEM microstructure of interfaces of a) AG50/SUS 430 interconnect and b) AG50/NiO–YSZ anode. The specimens were treated at 750 °C for 2 h in air.

the components or oxide scale, resulting in a gradual increase in the leak rate. However, the damage accumulated over 6 thermal cycles did not reach the extent that can adversely affect the OCV.

4. Conclusions

Al_2O_3–glass composite seals of various glass contents were fabricated by tape casting, and their leak rates were measured under different temperatures, gas pressures and compressive loads. The seal with optimized glass content was subjected to thermal cycling and single-cell tests to further demonstrate the viability of the seal. From the results obtained, the following conclusions are drawn.

1) The sealing performance is improved with the increase of glass content in the composite seal due to the coalescence of glass particles and the glass encapsulation of Al_2O_3 particles to densify the seal microstructure. The optimized composition for the seal is 50 wt% glass (AG50), which presents an extremely low leak rate and avoids the possible seal breakage caused by microstructure densification upon operation.
2) Increasing the testing gas pressure or decreasing the testing temperature and compressive load increases the leak rate of the AG50 seal; however, the highest leak rate measured (0.016 sccm cm^{-1}) is far below the conventionally accepted level. The AG50 seal can withstand at least 25 thermal cycles between 750 and 200 °C without exhibiting dramatic leaking performance degradation.
3) Using the AG50 seal, a 10 × 10 cm^2 anode-supported single cell (active area of 9 × 9 cm^2) can achieve a high initial OCV of 1.18 V. Its OCV after thermal cycling is in the range of 1.16 and 1.19 V, which demonstrates the applicability of the AG50 seal in practical SOFC operations.

Acknowledgments

This research was financially supported by the National “863” program (2011AA050702), and Hubei Province Innovation Team Project (2008CDA004). The SEM and XRD characterizations were performed with the assistance of the Analytical and Testing Center of Huazhong University of Science and Technology.

References

[1] S.C. Singhal, K. Kendall, High Temperature Solid Oxide Fuel Cells: Fundamentals, Design and Applications, Elsevier Advanced Technology, Netherlands, 2003.
[2] S.C. Singhal, J. Mizusaki (Eds.), Solid Oxide Fuel Cells-IX, The Electrochemical Society Proceedings, Pennington, NJ, 2005.
[3] J.P.P. Huijsmans, F.P.F. van Berkel, G.M. Christie, J. Power Sources 71 (1988) 107–110.
[4] S. Le, K. Sun, N. Zhang, M. An, D. Zhou, J. Zhang, D. Li, J. Power Sources 161 (2006) 901–906.
[5] R.N. Singh, Int. J. Appl. Ceram. Technol. 4 (2007) 134–144.
[6] J.W. Fergus, J. Power Sources 147 (2005) 46–57.
[7] S.P. Simner, J.W. Stevenson, J. Power Sources 102 (2001) 310–316.
[8] W. Liu, X. Sun, M. Khaleel, J. Power Sources 185 (2008) 1193–1200.
[9] M.K. Mahapatra, K. Lu, Mater. Sci. Eng. R Rep. 67 (2010) 65–85.
[10] K.A. Nielsen, M. Solvang, S.B.L. Nielsen, A.R. Dinesen, D. Beeaff, P.H. Larsen, J. Eur. Ceram. Soc. 27 (2007) 1817–1822.
[11] J. Milhans, S. Ahzi, H. Garmestani, M.A. Khaleel, X. Sun, B.J. Koeppel, Mater. Des. 30 (2009) 1667–1673.
[12] E.V. Stephens, J.S. Vetrano, B.J. Koeppel, Y. Chou, X. Sun, M.A. Khaleel, J. Power Sources 193 (2009) 625–631.
[13] W.N. Liu, X. Sun, M.A. Khaleel, J. Power Sources 196 (2011) 1750–1761.
[14] W.N. Liu, X. Sun, B. Koeppel, M. Khaleel, Int. J. Appl. Ceram. Technol. 7 (2010) 22–29.
[15] T. Zhang, Q. Zou, J. Zhang, D. Tang, H. Yang, J. Power Sources 204 (2012) 122–126.
[16] N. Govindaraju, W.N. Liu, X. Sun, P. Singh, R.N. Singh, J. Power Sources 190 (2009) 476–484.

[17] Y.S. Chou, J.W. Stevenson, P. Singh, J. Power Sources 152 (2005) 168–174.
[18] M. Bram, S. Reckers, P. Drinovac, J. Mönch, R.W. Steinbrech, H.P. Buchkremer, D. Stöver, J. Power Sources 138 (2004) 111–119.
[19] Z.G. Yang, G.G. X, K. Meinhardt, K. Weil, J. Stevenson, Chemical Stability of Glass Seal Interfaces in Intermediate Temperature Solid Oxide Fuel Cells, Springer, Germany, 2004.
[20] S. Sang, W. Li, J. Pu, J. Li, J. Power Sources 177 (2008) 77–82.
[21] Z. Dai, J. Pu, D. Yan, B. Chi, J. Li, Int. J. Hydrogen Energy 36 (2011) 3131–3137.
[22] Y.N. Ye, D. Yan, X.P. Wang, J. Pu, B. Chi, J. Li, Int. J. Hydrogen Energy (2011) 1–7.
[23] S.B. Sang, J. Pu, S.P. Jiang, J. Li, J. Power Sources 182 (2008) 141–144.
[24] J. Pu, J. Li, B. Hua, G.Y. Xie, J. Power Sources 158 (1) (2006) 354–360.